Pharm Res (2013) 30:225–237
DOI 10.1007/s11095-012-0865-7

RESEARCH PAPER

Continuous Generation of Ethyl Cellulose Drug Delivery Nanocarriers from Microbubbles

Oguzhan Gunduz • Zeeshan Ahmad • Eleanor Stride • Mohan Edirisinghe

Received: 21 June 2012 / Accepted: 13 August 2012 / Published online: 6 September 2012
© Springer Science+Business Media, LLC 2012

ABSTRACT

Purpose To investigate a new microfluidic method for the continuous preparation of hollow-shell nanoparticles of a hydrophobic polymer and the simultaneous encapsulation within these of a hydrophilic active pharmaceutical ingredient.

Method A specially designed and constructed microfluidic device which facilitates at a junction the impingement of two liquids flowing in capillaries kept 60° apart, one containing the polymer ethyl cellulose (EC) and the other active pharmaceutical ingredient amoxicillin, and a gas flowing in a capillary bisecting the two liquid flows, was used to continuously generate EC coated microbubbles at an outlet directly below the gas flow. The bubbles produce EC nanoparticles whilst encapsulating amoxicillin, and these were characterised by microscopy, zeta potential measurements, FTIR and UV spectroscopy and *in vitro* drug release and kinetic studies.

Results The device produced $\sim 5 \times 10^6$ microbubbles per minute from the surface of which EC nanocarriers were released spontaneously according to an evaporation-controlled mechanism. The gas pressure was very effective in controlling the size and size distribution of the nanocarriers.

Conclusions Nanocarriers with diameter between 10 and 800 nm were continuously produced by controlling the gas pressure between 110 and 510 kPa. Depending on their size, particles were capable of encapsulating 65–88% of amoxicillin which was released over ~12 h.

KEY WORDS bubbles · drug delivery · microfluidic · nanocarriers

INTRODUCTION

Microfluidics deals with the movement of small volumes of fluids in capillaries of several hundred or tens of micrometres in diameter. In the last decade, these technologies have advanced significantly largely facilitated by progress in the electronics industry (1). Recently, the applications of microfluidics have been considerably expanded to include the multidisciplinary fields of biotechnology, such as DNA analysis (1–3), polymerase chain reaction (1,2), protein crystallisation high-throughput screening (2) and cell culture (3). Microfluidic systems have also been used to produce micro- and nanoparticles with excellent control of composition and morphology, as well size and size distribution. As-generated products can be solidified downstream either thermally or chemically (1,4).

Micro/nanoparticles are widely used in drug delivery systems for small drug molecules in addition to macromolecules such as proteins and hormones (5). Nanoparticles comprising biodegradable or biocompatible polymers show some advantages over liposomes of similar size in terms of

Electronic supplementary material The online version of this article (doi:10.1007/s11095-012-0865-7) contains supplementary material, which is available to authorized users.

O. Gunduz • E. Stride • M. Edirisinghe (✉)
Department of Mechanical Engineering, University College London
Torrington Place
London WC1E 7JE, UK
e-mail: m.edirisinghe@ucl.ac.uk

O. Gunduz
Materials Department, Technical Education Faculty
Marmara University
Goztepe
Istanbul 34722, Turkey

Z. Ahmad
School of Pharmacy and Biomedical Sciences
University of Portsmouth
St. Michaels Building, White Swan Road
Portsmouth PO1 2DT, UK

E. Stride
Institute of Biomedical Engineering, Department of Engineering Science
University of Oxford
Old Road Campus
Oxford OX3 7DQ, UK

stability both during storage and *in vivo* (6). They may involve either a polymeric matrix (nanospheres) or a reservoir system in which an oily or aqueous core is enclosed by a thin polymeric wall (nanocapsules) (6). Fabrication of polymer particles is most commonly based on precipitation, produced using solvent removal (e.g. by evaporation) or anti-solvent addition. Liquid anti-solvent methods are widely used in industry. These methods have the advantage of not involving any chemical reactions, since only physical processes occur during the precipitation of the solute (7). Thus, the starting material can simply be the selected polymer dissolved in a solvent. Due to fast micromixing effects enabled by microfluidics, microscale liquid/liquid anti-solvent and evaporation processes provide an efficient technique for generating polymer nanoparticles with well-controlled size distribution.

Monodispersivity is very important for microcapsules used in drug delivery systems, because the distribution of microcapsules *in-vivo*, and the interaction with biological cells, is significantly affected by particle size (6,8). Monodisperse microcapsules can enhance bioavailability and limit unwanted side-effects (6). Also particle size and the surface characteristics of nanoparticles can be simply controlled to accomplish both passive and active drug targeting after parenteral administration (6).

We have selected amoxcillin (AMX), chosen as a model drug because an oral sustained-release formulation for amoxicillin could increase the period of active drug absorption in the extracellular fluid, thus extending the dosing interval while ensuring antimicrobial activity. This reasoning is based on the pharmacodynamic properties of the drug (9). Several mathematical models have been proposed for the analysis of drug release processes and mechanisms. These models are generally case specific, but could be merged to simultaneously take account of several factors such as drug carrier characteristics (polydispersivity, physical properties, morphology etc.) providing kinetic data of multi-parameter systems, which are often not readily available from experiments (10). The most commonly used models are those based on relatively simple and easy to use mathematical approaches. Among these, the Higuchi's model, which enables the prediction of release rates with good accuracy in most cases, is frequently used (11).

Ethyl cellulose (EC) is widely used as a dissolution rate-controlling polymer in sustained-release dosage forms (12). EC is a non-toxic, stable, compressible, passive, hydrophobic polymer that has been commonly utilized to prepare pharmaceutical dosage forms, even though it is not a biodegradable polymer, because of its non-toxicity, good stability, ease of processing and low cost (13). The properties of ethyl cellulose sustained release products, including film coated tablets, microspheres, microcapsules and matrix tablets for both soluble and poorly soluble drugs have been reported (14). EC is used for microencapsulation of various pharmaceuticals to stabilize them against unwanted interactions. It has been used as a polymeric coating, for controlled release in oral preparations, in transdermal films and patches, pharmaceutically useful aqueous latex dispersions, and as a particle emulsion stabilizer (15,16).

In previous work, EC microparticles have commonly been prepared using a variety of techniques such as spray drying (17), coacervation (18), emulsion solvent evaporation (ESE) (9,18), super-critical anti-solvent technique (SAS) (18,19), precision particle fabrication (PPF) (20) and microfluidics (8). Kang and Kim (17) prepared EC microparticles containing alginate and calcium carbonate nano-particles by spray drying water-oil emulsions. Most of these particles were several to tens of micrometre in size and irregular in shape (17). Khan *et al.* (21) prepared EC microparticles for sustained release of nimesulide by coacervation and studied the influence of various variables, on the drug to polymer ratio and also the drug-polymer compatibility. The recovery of microspheres from EC solutions was found to be difficult and those recovered were agglomerated due to the presence of residual EC. This is also a problem in EC microspheres of size 10–100 μm prepared by spray drying. Song *et al.* (9) prepared amoxicillin filled EC microcapsules by the ESE method and these were of diameter 342–574 μm. Montes *et al.* (19) used the SAS technique to prepare microparticles of EC and amoxicillin with precipitation using CO_2. Microparticles of EC in the range 3.8–5.0 μm were obtained. However, these particles formed agglomerates and also this technique involves many steps. The PFF technique studied by Choy and co-workers (20), was shown to have the capacity to prepare uniform solid EC microparticles with diameters of 35–90 μm. More recently, microfluidic systems have also been used to produce micro/nanoparticles with controlled size distributions. Lui *et al.* (8) successfully utilized templates to generate EC hollow particles using a microfluidic device obtaining an average diameter of 137 μm. In comparison with other methods the distinct advantage of the microfluidic method is the ability to generate near-monodisperse (very narrow size distribution) products continuously. The geometry of the microfluidic junction can also be changed to accommodate the simultaneous flow of many liquid and gas streams, which allows the composition, size, and morphology of the products to be varied.

In this work we have processed EC solutions using a novel V-junction microfluidic (VJM) device to generate microbubbles and the subsequent break-up of the bubble surface produces polymer nanoparticles with near-uniform size, shape and structure. The nanoparticles are also able to encapsulate an active pharmaceutical ingredient simultaneously fed into the device. This approach

described here could be very useful in the controlled production of nanoparticles for biotechnology or therapeutic applications. This method proposed in this study can also be adapted to fabricate other biocompatible and biodegradable microcapsules/nanoparticles from polymers such as poly (lactic acid-co-glycolic acid), polylactic acid and polycaprolactone which have numerous biomedical applications.

MATERIALS AND METHODS

Materials and Solutions

EC powder (molecular weight: 40,000 g/mol, Sigma-Aldrich, Poole, UK) was used and consists of porous irregular particles >100 µm in size (Fig. 1a). Acicular powder particles of commercial amoxicillin (AMX, molecular

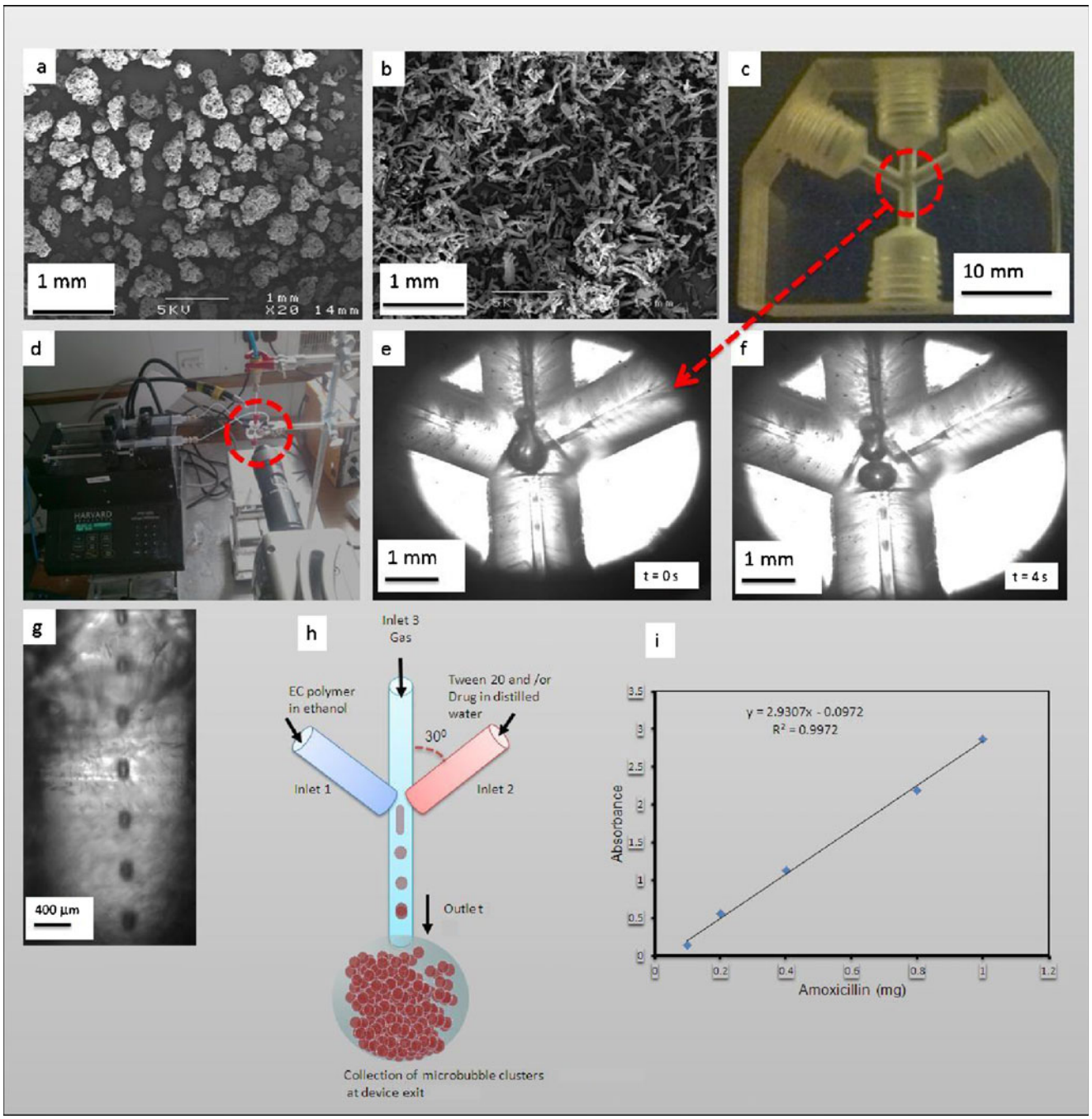

Fig. 1 SEM images of (**a**) unprocessed ethyl cellulose, (**b**) unprocessed AMX. (**c**) the VJM device used, (**d**) experimental equipment set-up (**e**) high-speed photographs showing the formation of microbubbles at $t=0$, (**f**) $t=4$ s, (**g**) high-speed camera image showing the bubbles at the outlet capillary, (**h**) schematic illustration of VJM device generating microbubbles, (**i**) calibration curve used to detect drug AMX in *in-vitro* study.

weight: 365.4 g/mol), which was used as the active pharmaceutical ingredient in this study (Fig. 1b) and Tween 20 viscous liquid (polyoxyethylenesorbitan monolaurate) were also obtained from Sigma-Aldrich. Ethanol was provided by BDH Laboratory Supplies UK and was used to prepare the EC solution. 5 wt.% of EC was dissolved in ethanol by magnetic stirring in a conical flask for 2000s at the ambient temperature (23°C). 2 wt.% of Tween 20 was dissolved in distilled water under identical conditions. Subsequently, 0.6 mg/ml of AMX was added to the 2 wt.% Tween 20 solution for the *in vitro* release study.

Characterization of Solvents and Solutions

The liquid physical properties, viscosity, surface tension and density were measured using calibrated equipment as follows. Viscosity was determined using a U-tube viscometer or a VISCOEASY rotational viscometer. Surface tension was measured using a Kruss Tensiometer. Density was measured using a standard 25 ml density bottle.

Device Design and Construction

A V-junction microfluidic (VJM) device (Fig. 1c) was designed and constructed. The device was fabricated using polymethylmethacrylate (PMMA) by Computer Numerical Control machining. Teflon fluorinated ethylene polypropylene (FEP) capillaries with internal diameter ID= 200 μm and outer diameter OD=1.6 mm were embedded in the PMMA block (22×27×15 mm). This device was found to be both robust and rigid, withstanding the high pressures generated during bubbling (up to 700 kPa).

Bubble Generation

Diagrams illustrating the generation of microbubbles are shown in Fig. 1d, e, f, g and h. Teflon FEP tube was used to connect the inlets and outlet of the microchannels, which were supplied with gas and the solutions. The top tube of the VJM device (inlet 3) was connected to a pressurised vessel supplying N_2 under controlled pressure. The gas pressure was controlled using a high-precision micrometering valve (British Oxygen Company, UK). Liquid was supplied from a 10 ml plastic syringe using digitally controlled syringe pumps (model PHD 4400, Harvard Apparatus, UK). The gas was introduced from the main channel and liquids from the two angled channels (30° to the vertical), respectively. These channels cross at a section where bubbles are formed and the resulting bubbles were collected from the outlet (fourth) capillary at the bottom of the device. The bubbles generate particles.

Bubble and Particle Characterization

The morphology and structure of the microbubbles and particles were determined using optical microscopy (Nikon Eclipse ME600) and scanning electron microscopy (Joel JSM-6301F field emission, SEM). In addition, the internal structure of the particles was also studied using SEM, in combination with a focused-ion-beam (FIB) microscope for preparing cross-sections of the particles (Carl Zeiss XB1540 "Cross-Beam"). All bubbles were collected on a glass slide with its surface coated with distilled water. The samples were dried under ambient conditions (23°C) in desiccators. Dried samples were sputter coated with gold for 180 s prior to SEM studies under an accelerating voltage of 5 kV.

Zeta Potential Measurement

Zeta potential was determined using a Malvern Nano-ZS analyser at 25°C. The measurements were repeated at least three times and were taken after allowing 120 s (equilibrium time).

FTIR Spectroscopy

FTIR spectroscopy (PerkinElmer Life and Analytical Sciences, Inc., Wellesley, MA, USA) on untreated pure EC and dried EC was performed after finely grinding a portion of each sample with potassium bromide (KBr), according to standard practice. The powder mixture was then moulded in a mechanical die press to form a translucent pellet through which the beam of the spectrometer could pass.

In Vitro Release and Kinetic Studies

A calibration graph (Fig. 1i) was prepared for AMX using a UV spectrometer (Lambda 35, Perkin Elmer,UK).

The AMX–polymer particles formed from the bubbles were subjected to *in vitro* release studies. Samples of the particles were collected in a glass vial in distilled water and kept at 37°C with continuous stirring. Distilled water was chosen because of the high solubility of AMX in it. To assess the release of AMX from generated particles, samples were centrifuged at 3,313 g for 30 min and the supernatant was removed and its absorbance was measured using the calibration graph, based on the absorbance peak area at a wavelength of 229 nm. The release assay was repeated 3 times to obtain the average value.

An accurately weighed sample of amoxicillin nanocapsules prepared in this work was powdered into a white suspension using a small volume of water and the AMX in the sample was assessed using UV spectrometry. The

following equations were utilised to evaluate yield and encapsulation efficiency as described by Song *et al.* (9) and also drug loading rate (22):

$$Yield = \frac{Weight\ of\ NC}{Total\ Weight\ of\ Material} \times 100$$

$$Encapsulation\ Efficiency = \frac{Weight\ of\ AMX\ in\ NC}{Weight\ of\ AMX\ Used} \times 100$$

$$Drug\ Loading = \frac{Weight\ of\ AMX\ in\ NC}{Total\ Weight\ of\ NC} \times 100$$

where *NC* = nanocapsules and *AMX* = *amoxicillin*

The AMX release curves were evaluated using the Higuchi model (11):

$$Q = k_h t^{1/2},$$

Q is the amount of drug released at time t and k_h is the Higuchi dissolution constant. Error bars represent the standard deviation from three repeat drug release experiments.

RESULTS AND DISCUSSION

Figure 1e, f and g shows high-speed camera images of the sequence of bubble generation in the device. The formation of bubbles in this way has been studied widely, both theoretically and experimentally, and it has been revealed that bubbles are formed *via* a "pinch-off" process due to the instability of the gas/liquid interface (23). As defined in earlier studies (24,25) relating to the preparation of bubbles from microfluidic devices, gas streams impinge upon the liquid flow at orifices of varying geometry and focuses into a jet. The gas pressure influences the diameter of the gas column, the break-up point and also the wavelength of the instability. These factors combined determine the eventual bubble size. The most vital solution properties affecting the generation of monodisperse microbubbles by our method are surface tension and viscosity and these can be varied by changing the polymer concentration (26).

Prior to the work described in this paper, several EC solutions were used to generate bubbles and these trial and error experiments showed that setting the EC concentration at 5 wt.% gave stable and controlled bubbling. 5 wt.% EC in ethanol (solution having a viscosity of 23 mPa s, density of 871 kg m^{-3} and surface tension of 39 mN m^{-1}) was therefore used in this work and injected through inlet 1. Tween 20/AMX solution was injected through inlet 2 (having a viscosity of 1.5 mPa s, density of 1,007 kg m^{-3} and surface tension of 38 mN m^{-1}). At the same time nitrogen gas was fed into the inlet 3. Bubbles were generated at different gas pressures of 110, 340, and 510 kPa, while inlet 1 and 2 flow rates were kept constant at 500 µl/min. This flow rate was selected to achieve continuous stable bubbling at the outlet of the VJM device, and was not changed in this work.

The process of bubble generation is further illustrated in the high-speed camera video (see Supplementary Material). The generation of EC particles from the bubbles is explained in Fig. 2. Firstly, as the ethanol in the bubble surface decreases due to its evaporation. As a result the concentration of hydrophobic EC content and water (absorbed in ethanol) increases. Thus, the solubility of EC decreases dramatically as the microbubbles nucleate and precipitates the "excess" EC in the form of particles at the bubble surface while the N_2 gas core is intact. The hydrophilic AMX is thereby encapsulated due to its uptake by the water. Subsequently, these EC particles consolidate and result in the formation of capsules.

Figure 3a, b and c shows optical images of microbubbles, in this case prepared with a gas pressure of 110 kPa, taken at different times following preparation. The as-prepared bubble diameter was in the range ~160–200 µm (Fig. 3d). The microbubbles in turn generated spherical solid EC nanoparticles ranging from 10 nm to 800 nm (Figs. 4, 5, 6 and 7).

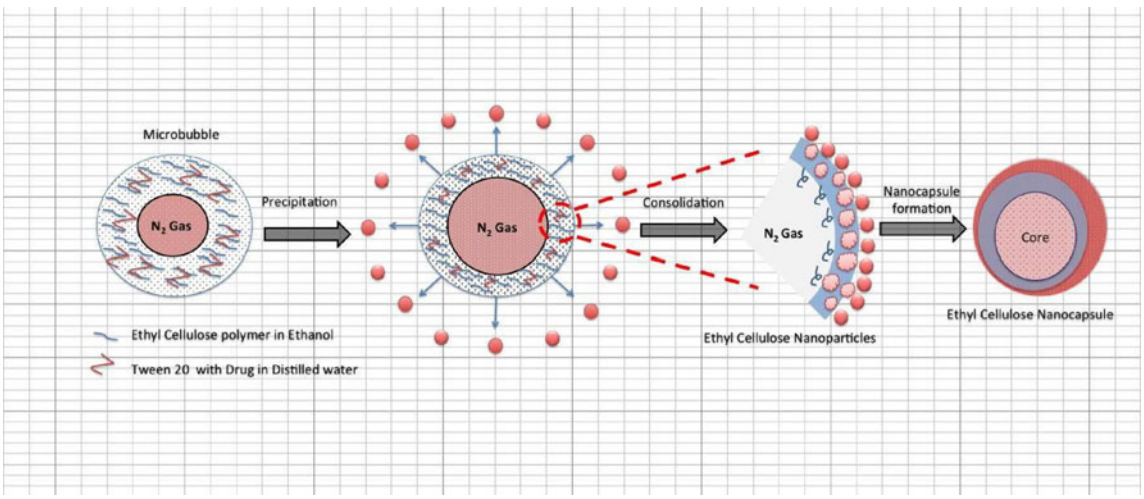

Fig. 2 Schematic diagram showing the evolution of microbubbles during the process of nanoparticle generation.

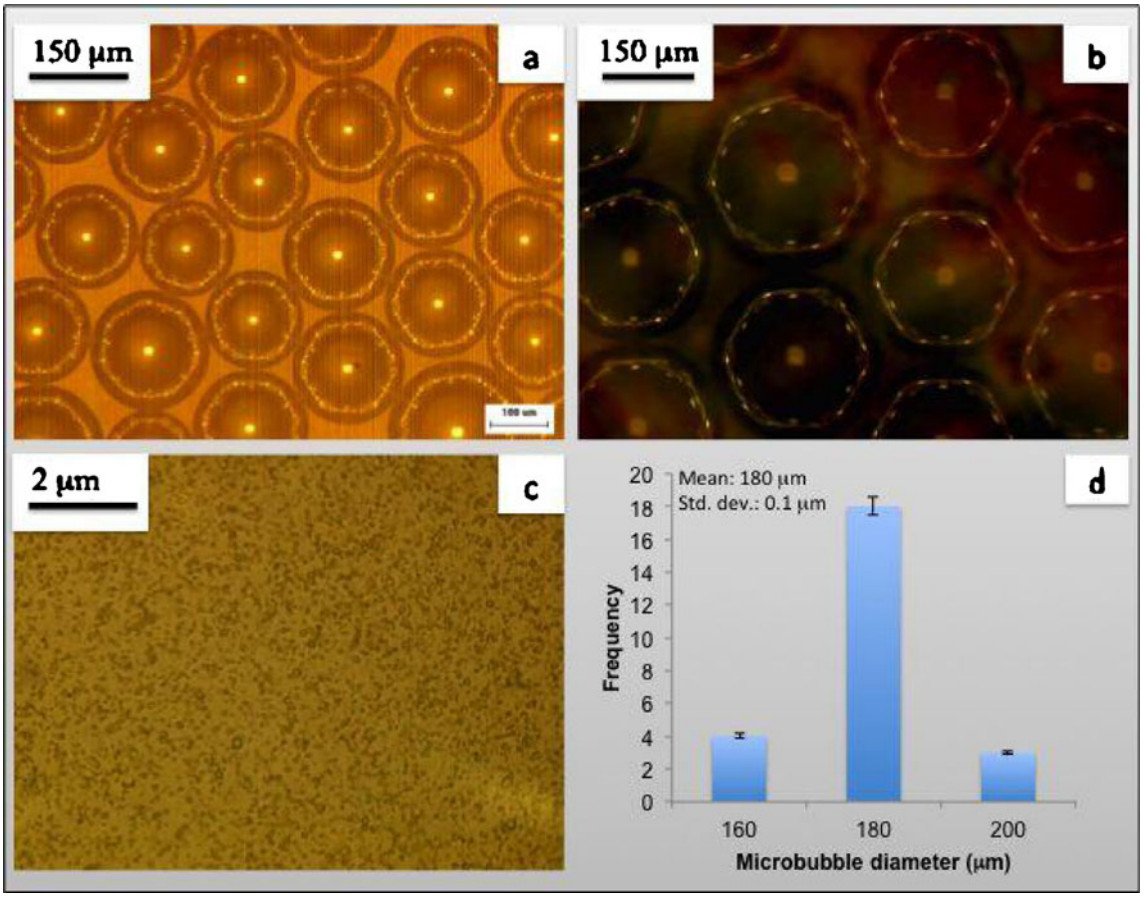

Fig. 3 Optical images of bubbles prepared with a gas pressure of 110 kPa taken at various times following preparation, (**a**) 30 s, (**b**) 120 s, (**c**) 24 h and (**d**) Microbubble size distribution of (**a**) determined from optical images.

The presence of Tween 20 prevented coalescence of the nanoparticles and unagglomerated batches of particles were obtained without any extra processing. Zeta potential was ~ −21 mV for the EC particles prepared at 110 kPa gas pressure and ~ −24.5 mV for the 510 kPa samples. Zeta potential measurements indicate the stability of the particles in the dispersion. The values obtained indicate that there was sufficient zeta potential to avoid coagulation and flocculation of the particles due to the addition of Tween 20. Increase of the Tween 20 content is likely to impart even more stability and increase the magnitude of the zeta potential further. However, the addition of surfactants in drug delivery formulations has to be kept to a minimum.

The size distribution of the EC particles produced could be tailored by varying the N_2 gas pressure (Fig. 4). Thus different sizes of nanoparticles were obtained when using gas pressures of 110, 340, and 510 kPa. This is thought to be linked to the fact that the stability of the bubbles generated at the higher pressures was also lower, with particle formation and bubble break up occurring much more rapidly (to the extent that the as prepared size distribution could not be reliably determined for the microbubbles prepared at 340 and 510 kPa).

Detailed analysis using SEM revealed that all nanoparticles were near-spherical with a smooth outer surface (Figs. 5a, b, 6a, b, 7a and b) and size distributions obtained are shown in Figs. 5c, 6c, and 7c. Thus, the polydispersivity of the nano particles prepared could also be tailored. The polydispersivity index (PI = standard deviation/mean size) of the particles prepared at all gas pressures (110, 340, and 510 kPa) were, in the range 16–17%. It is noteworthy that at a pressure of 510 kPa all the particles generated were <100 nm.

The internal morphology of these nanospheres (Fig. 8a) were revealed by the FIB study. SEM close-up images of the thin-sliced EC particles are shown in Fig. 8b and c. This showed that the particles had a hollow internal structure (Fig. 8d). Thus, for a capsule of ~800 nm the shell thickness was 290 nm. The hollow structure is consistent with the particle generation, precipitation, consolidation and nanocapsule formation model presented in Fig. 2.

At 500 µl/min EC solution and Tween 20 flow rates and the 510 kPa gas pressure, a production rate of ~5,230

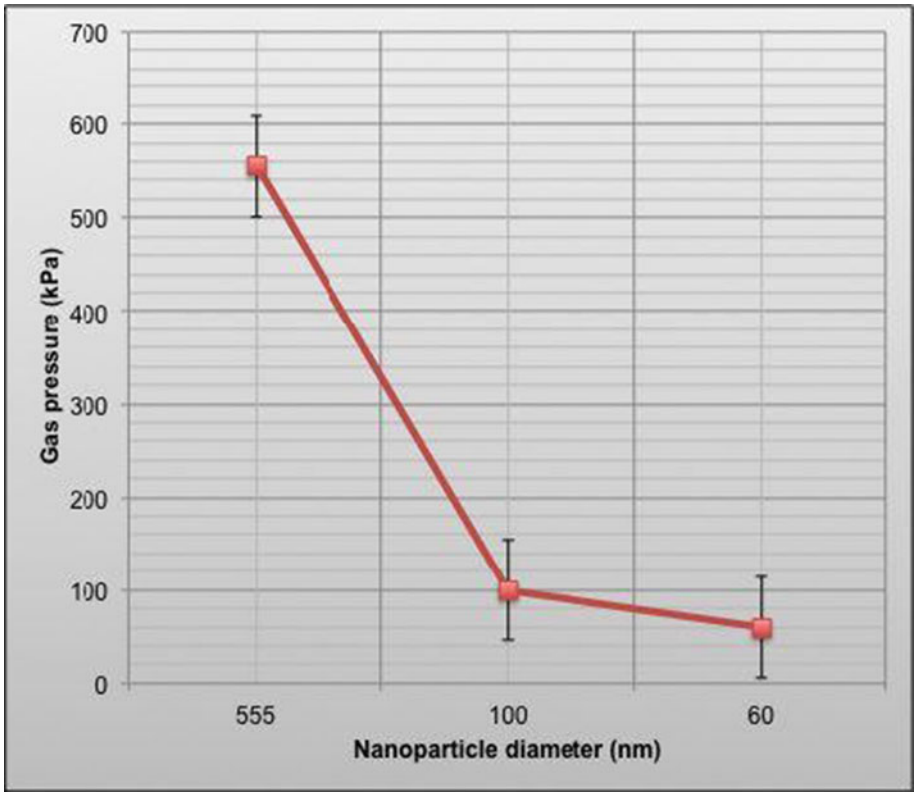

Fig. 4 Size of nanoparticles as a function of gas pressure (error bars show standard deviation of the diameter).

bubbles per minute was observed. Thirty independent measurements were made from video recordings to determine this. This gives a production rate of $\sim 5 \times 10^6$ nanoparticles per minute.

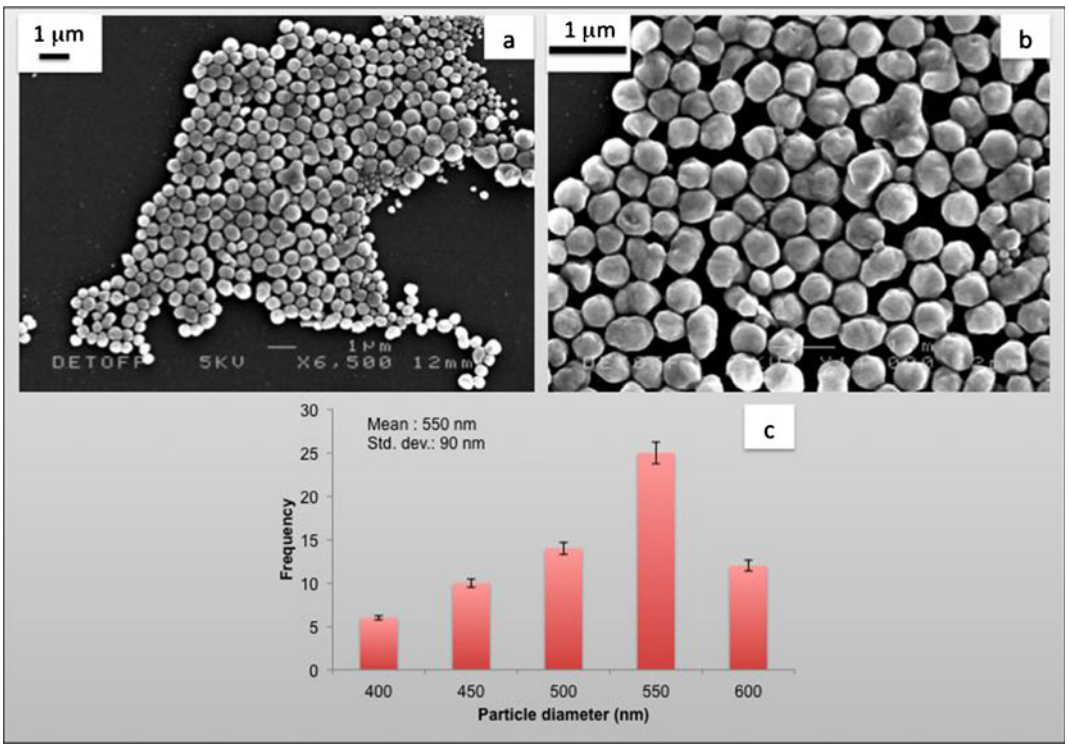

Fig. 5 SEM images of nanoparticles prepared at a gas pressure of 110 kPa and a flow rate of 500 μl/min. (**a**) Low magnification, (**b**) high magnification and (**c**) histograms showing nanoparticle size distributions calculated from SEM images.

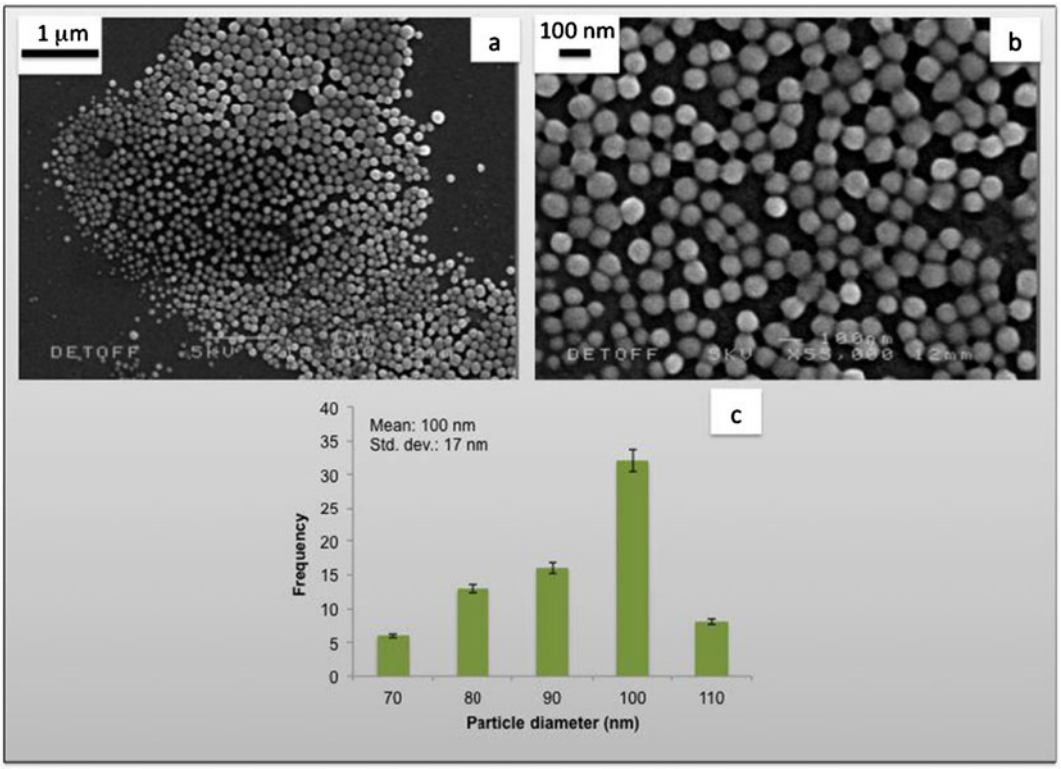

Fig. 6 SEM images of nanoparticles prepared at a gas pressure of 340 kPa and a flow rate of 500 μl/min. (**a**) Low magnification, (**b**) high magnification and (**c**) histograms showing nanoparticle size distributions calculated from SEM images.

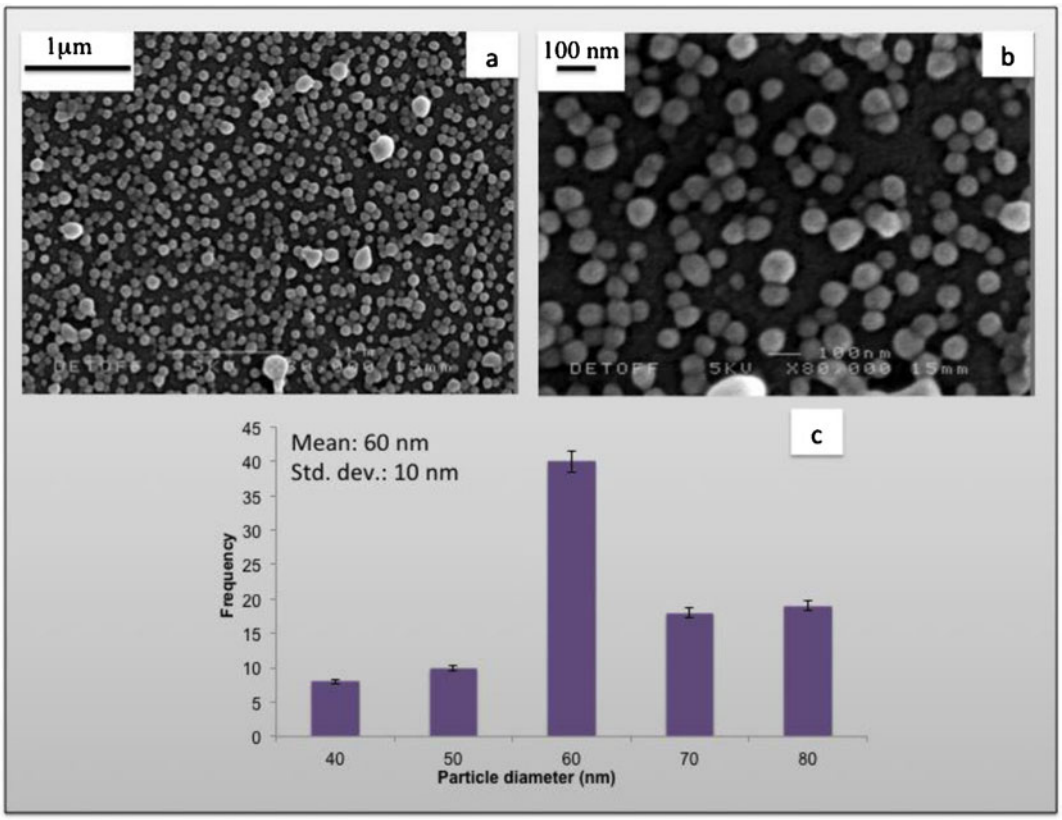

Fig. 7 SEM images of nanoparticles prepared at a gas pressure of 510 kPa and a flow rate of 500 μl/min. (**a**) Low magnification, (**b**) high magnification and (**c**) histograms showing nanoparticle size distributions calculated from SEM images.

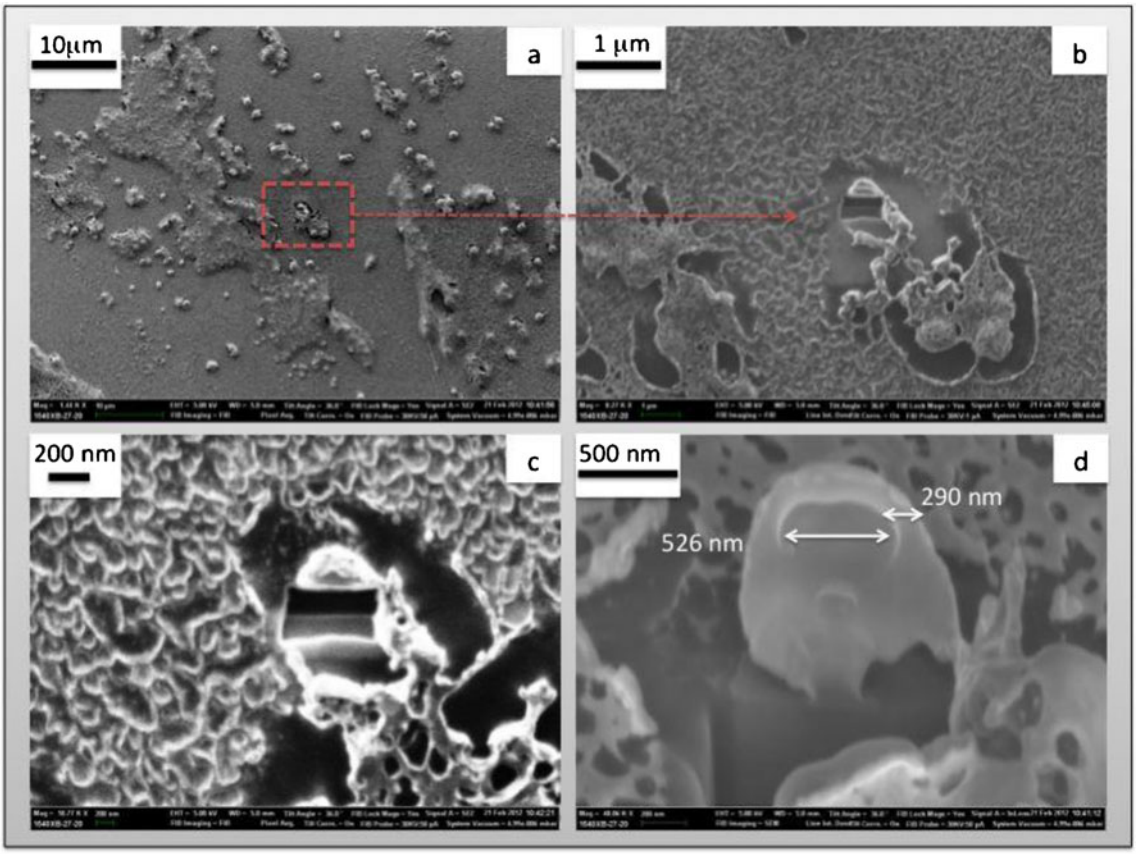

Fig. 8 FIB images showing the cross-section of EC particles prepared (**a**) low magnification, (**b**) top view EC particle, (**c**) close-up image, (**d**) particle with a thickness of 290 nm and hollow size of 526 nm.

FTIR spectra confirmed the composition of the nanoparticles Fig. 9 shows infrared spectra of samples of pure EC powder, and the dried EC sample over the wavenumber range 950 to 4,000 cm^{-1}. The spectrum of

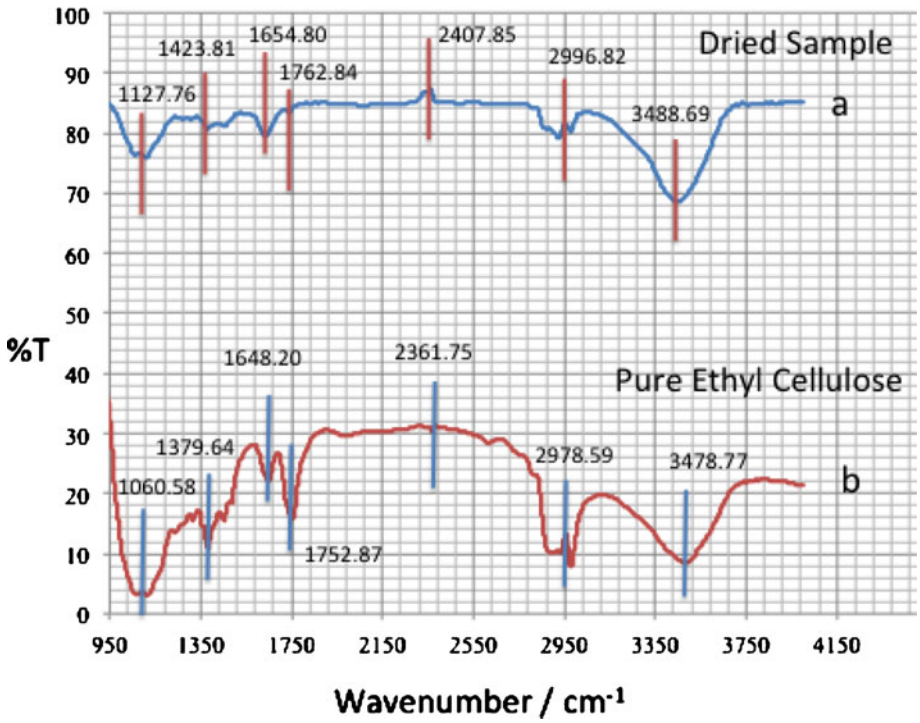

Fig. 9 FTIR spectra of ethyl cellulose sample and pure ethyl cellulose.

ethyl cellulose shows characteristic absorption bands for –C–O–C– stretching vibration at 1,060 cm^{-1} and C–H stretching bands at 2,970 cm^{-1}. The absorption at 1,376 cm^{-1} corresponds to C–H bending and also the spectrum for EC also demonstrated a distinct peak at about 3,464 cm^{-1}, which is due to the OH groups (27). The peak at 3478.77 cm^{-1} corresponding to –OH stretching/vibration changes slightly to 3488.69 cm^{-1} in the dried sample. This peak is also slightly wider and these changes are caused by the small amount of Tween 20 in the EC solution.

Two contrasting particles sizes shown in Figs. 5 and 7 were studied for API encapsulation and release studies. All of the AMX encapsulation experiments led to the successful preparation of unagglomerated drug-loaded EC particles similar to the findings of the experiments generating virgin EC particles. Therefore, using our device API can be loaded in the EC nanocapsules without agglomeration. The yield and encapsulation efficiency, respectively, were 87%, 65% for the 550 nm particles (Fig. 5) and 89%, 88%, for the 60 nm particles (Fig. 7). Furthermore, drug loading was ~13% for the 0.6 mg/ml of AMX used. This value can be varied by using higher AMX concentrations in the processing and forming stage. Kalogiannis *et al.* (28) have reported that the encapsulation of AMX in PLLA microparticles using the solution-enhanced dispersion by supercritical fluids (SEDS) process gave an encapsulation efficiency of 24–39%, while varying the AMX between 1 and 4 g/L. In our work, a lower percentage of AMX was used but our process gives higher encapsulation efficiency and this is a significant advantage.

Figures 10a and b also show SEM micrographs of the API nanocapsules after *in vitro* studies. The release profiles (Fig. 11) demonstrate a diffusion-based release mechanism, resulting in zero-order release of AMX from the resultant particles post burst release. Both particles show an initial (burst) release (~25 min) probably due to AMX at the surface of the nanoparticles followed by almost the same rate of AMX release over ~12 h. As expected, the total amount of AMX released tallied almost exactly with the encapsulation efficiency. In general, smaller particles

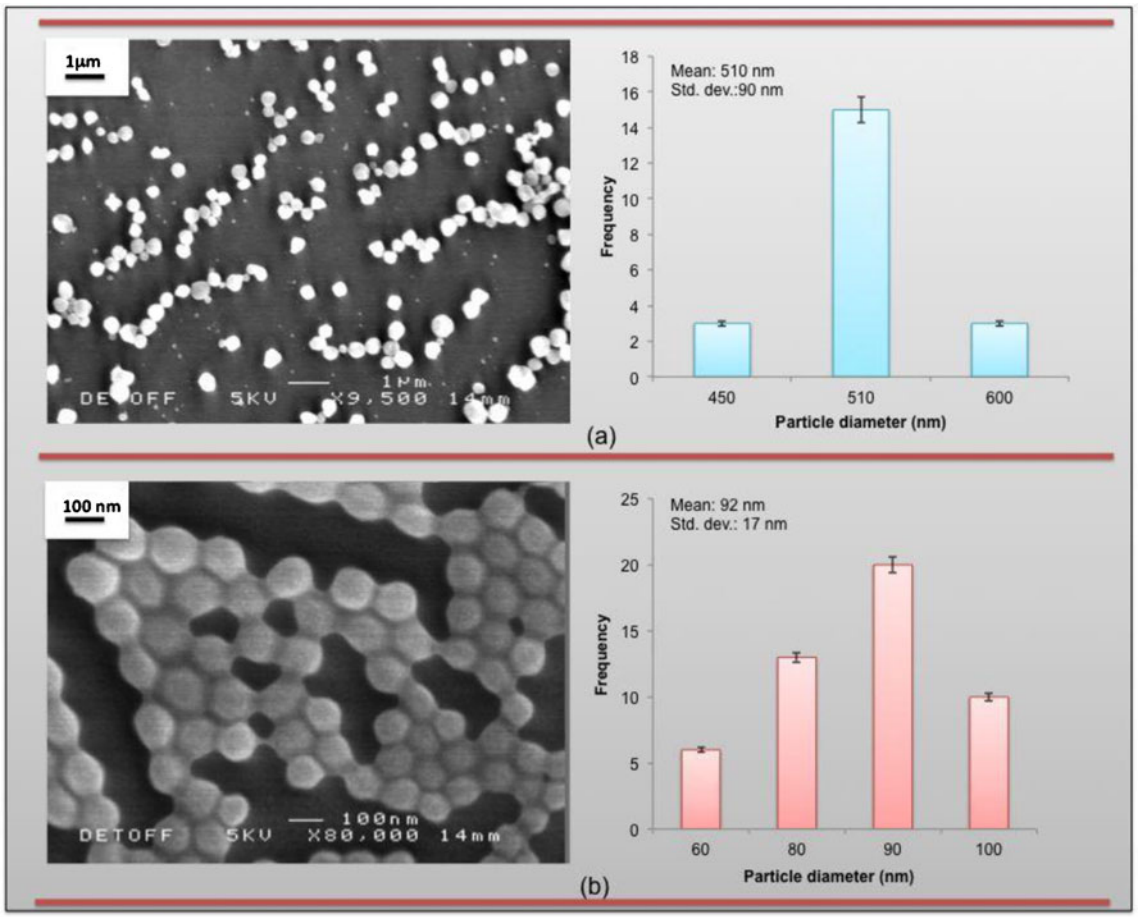

Fig. 10 SEM pictures of AMX-loaded nanocapsule samples prepared at a pressure gas pressure of (**a**) 110 kPa and (**b**) 510 kPa after release analysis and histograms showing size distributions after release calculated from SEM images. Typical size distributions before release are given in Figs. 5 and 7, respectively.

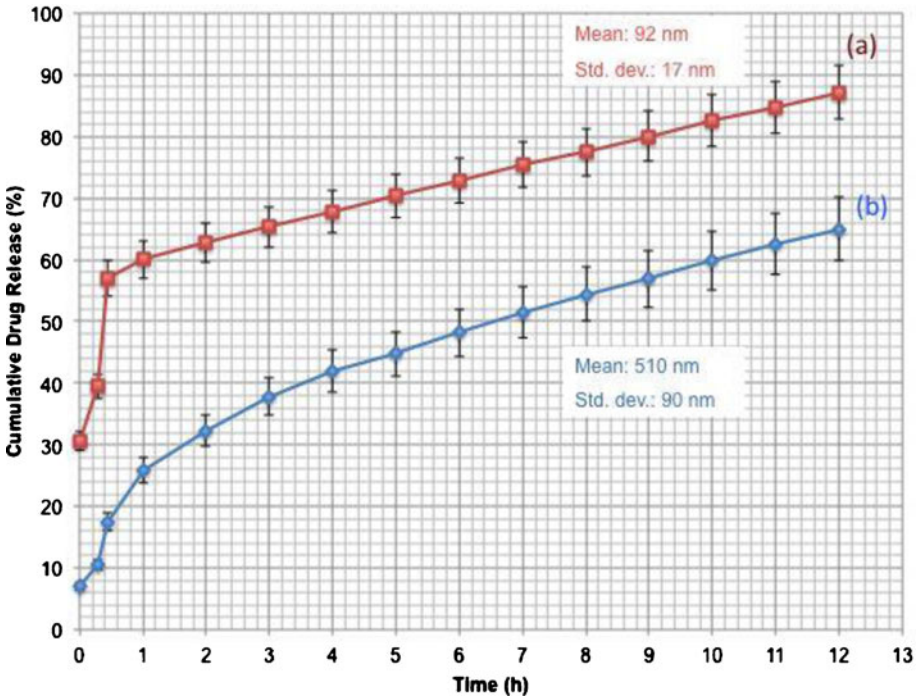

Fig. 11 Amoxicillin release profiles generated using particles shown in Fig. 10a and b.

release drug more rapidly than larger particles and also monodisperse particles release drug more slowly than polydisperse particles of similar average size (29). In Fig. 11, the particles compared have similar PI values but the mean size differs by almost five times, and this explains the trend observed. The results of the drug release pattern indicate that the release of small amounts of the AMX achieved the objective of having a sustained release dosing protocol for clinical use (30). However, the ability to speed-up AMX release is also facilitated by the use of finer particles (Fig. 11a as opposed to 11b). Release of AMX from the EC particles shows a good fit to the Higuchi model (Fig. 12), post burst release. The K_h values are 27 $h^{-1/2}$ and 19 $h^{-1/2}$ for the results obtained at 110 kPa and 510 kPa respectively, very similar to those results of Higuchi fit of other workers (31–33). This indicates that the release of AMX from the EC particles post burst release occurs mainly by diffusion, which is not surprising given the structure of the nanocapsule described earlier.

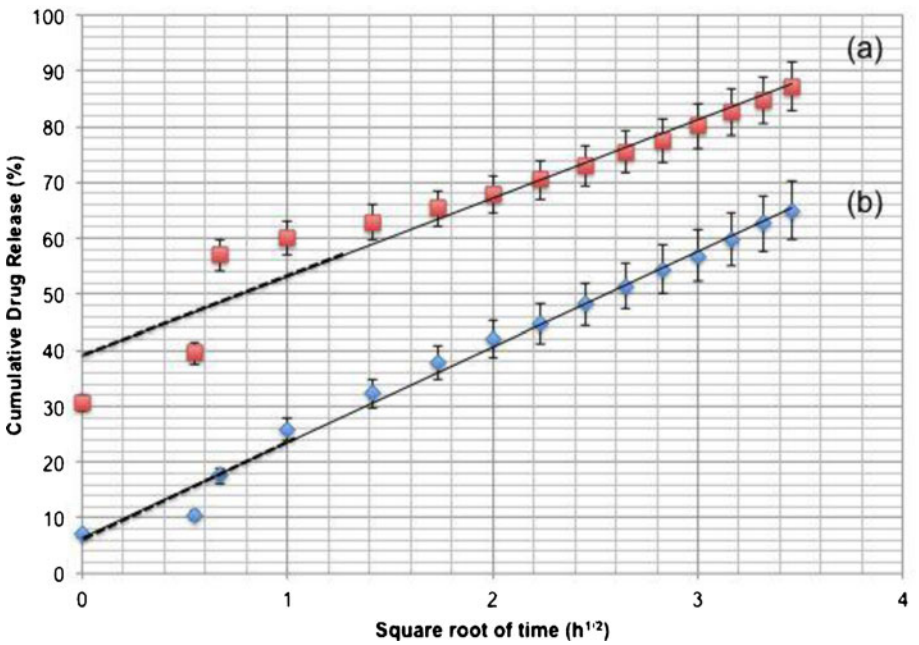

Fig. 12 Drug-release data in Fig. 11 fitted to the Higuchi model. Regression coefficient for (**a**) R^2: 0.925, and (**b**) R^2: 0.991.

CONCLUSIONS

Using a simple microfluidic V-junction device near-monodisperse polymer coated microbubbles were generated and from these hydrophobic polymer nanoparticles, in this instance ethylcellulose, were produced continuously at a rate of $\sim 5 \times 10^6$ per minute. It has been shown that these particles can be used as nanocarriers for a hydrophilic drug such an amoxicillin. The gas pressure has a significant effect on the nanocarrier diameter, thus we are able to control the diameter of nanocarrier between 10 and 800 nm. Encapsulation efficiency was in the range 65–88%, increasing with decreasing particle diameter and the drug-loading was ~13%. AMX release studies showed an initial burst release followed by gradual diffusion controlled (Higuchi) release over 12 h of all the AMX encapsulated. The smaller nanocarriers released AMX much faster at the outset. The present work demonstrates that this device and method is very successful for the encapsulation and subsequent release of a hydrophilic drug in a hydrophobic polymer carrier. Work to extend our method to hydrophilic carriers and hydrophobic drugs is progress at present.

ACKNOWLEDGMENTS AND DISCLOSURES

The authors wish to thank the Islamic Development Bank for supporting the doctoral research programme of Oguzhan Gunduz. They would also like to thank Kevin Reeves for the help with the scanning electron microscopes in the Archaeology Department at UCL and Dr Suguo Huo of the London Centre for Nanotechnology for the use of FIB.

REFERENCES

1. Dendukuri D, Doyle PS. The synthesis and assembly of polymeric microparticles using microfluidics. Adv Mater. 2009;21:1–16.
2. Zhang C, Xu J, Ma W, Zheng W. PCR microfluidic devices for DNA amplification. Biotech Adv. 2006;24:243–84.
3. Zheng B, Tice JD, Roach LS, Ismagilov RF. A droplet-based, composite PDMS/glass capillary microfluidic system for evaluating protein crystallization conditions by microbatch and vapor-diffusion methods with on-chip x-ray diffraction. Angew Chem Int Ed. 2004;43:2508–11.
4. Fang A, Cathala B. Smart swelling biopolymer microparticles by a microfluidic approach: synthesis, *in situ* encapsulation and controlled release. Coll Surf B: Biointerfaces. 2011;82:81–6.
5. Hung L-H, Teh S-Y, Jester J, Lee AP. PLGA micro/nanosphere synthesis by droplet microfluidic solvent evaporation and extraction approaches. Lab Chip. 2010;10:1820–5.
6. Barratt G. Colloidal drug carriers: achievements and perspectives. Cell Mol Life Sci. 2003;60:21–37.
7. Reverchon E. Supercritical antisolvent precipitation of micro- and nano- particles. J Supercrit Fluids. 1999;15:1–21.
8. Lui L, Yang J-P, Ju X-J, Xie R, Yang L, Liang B, *et al.* Microfluidic preparation of monodisperse ethyl cellulose hollow microcapsules with non-toxic solvent. J Coll Interf Sci. 2009;336:100–6.
9. Song M, Li N, Sun S, Tiedt LR, Liebenberg W, de Villiers MM. Effect of viscosity and concentration of wall former, emulsifier and pore-inducer on the properties of amoxicillin microcapsules prepared by emulsion solvent evaporation. Il Farmaco. 2005;60:261–7.
10. Siepmann J, Peppas NA. Higuchi equation: derivation, applications, use and misuse. Int J Pharm. 2011;418:6–12.
11. Higuchi T. Mechanism of sustained- action medication Theoretical analysis of rate of release of solid drugs dispersed in solid matrices. J Pharm Sci. 1963;52:1145–9.
12. Parikh NH, Porter SC, Rohera BD. Aqueous ethylcellulose dispersion of ethylcellulose. I. Evaluation of coating process variables. Pharmaceut Res. 1993;10:525–34.
13. Lin W-J, Wu T-L. Modification of the initial release of a highly water-soluble drug from ethyl cellulose microspheres. J Microencapsul. 1999;16:639–46.
14. Crowley MM, Schroeder B, Fredersdorf A, Obara S, Talarico M, Kucera S, *et al.* Physcochemical properties and mechanism of drug release from ethyl cellulose matrix tablets prepared by direct compression and hot-melt extrusion. Int J Pharm. 2004;269:509–22.
15. Bruno L, Kasapis S, Chaudhary V, Chow KT, Heng PWS, Leong LP. Temperature and time effects on the structural properties of a non-aqueous ethyl cellulose drug delivery system. Carb Poly. 2011;86:644–51.
16. Appel LE, Zentner GM. Use of modified ethycellulose lattices for microporous coating of osmotic tablets. Pharmaceut Res. 1991;8:600–4.
17. Kang MK, Kim J-C. pH-dependent release from ethylcellulose microparticles containing alginate and calcium carbonate. Coll Poly Sci. 2010;288:265–270.
18. Murtaza G. Ethylcellulose microparticles: a review. Acta Poloniae Pharm Drug Res. 2012;69:11–22.
19. Montes A, Gordillo MD, Pereyra EJ, de la Ossa M. Co-precipitation of amoxicillin and ethyl cellulose microparticles by supercritical antisolvent process. J Supercrit Fluids. 2011;60:75–80.
20. Choy YB, Choi H, Kim K. Uniform ethyl cellulose microspheres of controlled sizes and polymer viscosities and their drug-release profiles. J Appl Polym Sci. 2009;112:850–7.
21. Khan SA, Ahmad M, Murtaza G, Aamir MN, Madni A, Kousar R, Minhas U. Development of a single combined microencapsulated formulation of allopurinol and nimesulide and investigation of their release behaviours. Ars Pharm. 2010;51:105–16.
22. Hu L, Liu W, Li L, Zhao J, Yang X. Preparation and *in vitro*, *in vivo* evaluation of clarithromycin microcapsules. J Basic Clin Pharm. 2011;2:1–9.
23. Pancholi K, Stride E, Edirisinghe M. Dynamics of bubble formation in highly viscous liquids. Langmuir. 2008;24:4388–93.
24. Gunduz O, Ahmad Z, Stride E, Tamerler C, Edirisinghe M. Bioinspired bubble design for particle generation. J Roy Soc Interface. 2012;9:389–95.
25. Gunduz O, Ahmad Z, Stride E, Edirisinghe M. A device for the fabrication of multifunctional particles from microbubble suspensions. J Mat Sci Eng C. 2012;32:1005–10.
26. Stride E, Pancholi K, Edirisinghe M, Samarasinghe S. Increasing the non-linear character of microbubble oscillations at low acoustic pressures. J Roy Soc Interface. 2008;5:807–11.
27. Huang L-Y, Yu D-G, Branford-White C, Zhu L-M. Sustained release of ethyl cellulose micro-particle drug delivery systems prepared using electrospraying. J Mater Sci. 2012;47:1372–7.
28. Kalogiannis CG, Michailof CM, Panayiotou CG. Microencapsulation of amoxicillin in poly(L-lactic acid) by supercritical antisolvent precipitation. Ind Eng Chem Res. 2006;45:8738–43.
29. Xu Q, Hashimoto M, Dang TT, Hoare T, Kohane DS, Whitesides GM, *et al.* Preparation of monodisperse biodegradable polymer microparticles using a microfluidic flow-focusing device for controlled drug delivery. Small. 2009;5:1575–81.

30. Moine P, Mazoit JX. Streptococcus pneumoniae pneumonia in mice: Optimal amoxicillin dosing predicted from a pharmacokinetic-pharmacodynamic model. J Pharmacol Exp Ther. 1999;291:1086–92.
31. Wagh SC, Kumar JS, Banerjee S. Development and evaluation of a novel extended release venlafaxine hydrochloride matrix tablets. J Pharm Res. 2012;5:2184–90.
32. Pahwa R, Chhabra L, Lamba AK, Jindal S, Rathour A. Formulation and *in-vitro* evaluation of effervescent floating tablets of an antiulcer agent. J Chem Pharm Res. 2012;4:1066–73.
33. Bohr A, Kristensen J, Dyas M, Edirisinghe M, Stride E. Release profile and characteristics of electrosprayed particles for oral delivery of a practically insoluble drug. J R Soc Interface. 2012. doi:10.1098/rsif.2012.0166.